A&A 417, 731–743 (2004)
DOI: 10.1051/0004-6361:20034181

Astronomy & Astrophysics

Properties of galactic B[e] supergiants

III. MWC 300⋆

A. S. Miroshnichenko[1,2], H. Levato[3], K. S. Bjorkman[1], M. Grosso[3], N. Manset[4], A. B. Men′shchikov[5,6], R. J. Rudy[7], D. K. Lynch[7], S. Mazuk[7], C. C. Venturini[7], R. C. Puetter[8], and R. B. Perry[9]

[1] Ritter Observatory, Dept. of Physics and Astronomy, University of Toledo, Toledo, OH 43606-3390, USA
[2] Central Astronomical Observatory of the Russian Academy of Sciences at Pulkovo, 196140 Saint-Petersburg, Russia
[3] Complejo Astronómico El Leoncito (CASLEO), Casilla de Correo 467, 5400 San Juan, Argentina
[4] CFHT Corporation, 65–1238 Mamalahoa Hwy, Kamuela, HI 96743, Hawaii, USA
[5] Max-Planck-Institut für Radioastronomie, Auf dem Hügel 69, 53121, Bonn, Germany
[6] Institute for Computational Astrophysics, Saint Mary's University, Halifax, NS B3H 3C3, Canada
[7] The Aerospace Corp. M2/266, PO Box 92957, Los Angeles, CA 90009, USA
[8] Center for Astrophysics and Space Science, University of California, San Diego, 0111, La Jolla, CA 92093, USA
[9] Earth and Space Science Support Office, M/S 160, NASA Langley Research Center, Hampton, VA 23681, USA

Received 12 August 2003 / Accepted 21 December 2003

Abstract. We present the results of optical and near-IR spectroscopic and mid-IR imaging observations of the emission-line star MWC 300. Its properties and evolutionary state are still under debate (a B[e] supergiant or a Herbig Be star). For the first time we detected radial velocity variations of the photospheric lines and found a correlation between them and those of the He I λ5876 Å line. Most of the pure emission lines had stable positions for nearly 20 years. New estimates of the object's luminosity ($\log L/L_\odot = 5.1 \pm 0.1$), distance ($D = 1.8 \pm 0.2$ kpc), and systemic velocity ($+26 \pm 2$ km s^{-1}) were derived. We found that both the circumstellar extinction in the disk-like dusty envelope and the interstellar extinction play a significant role in the attenuation of the stellar brightness. Our 2D modeling of the observed spectral energy distribution in the wavelength range from 0.3 μm to 1.3 mm suggests that the star is viewed through a gaseous-and-dusty flared disk with an opening angle of 30°, an inclination angle of 10°, an equatorial optical depth $\tau_V = 3.0$, and a total mass of 0.08 $M_\odot$. We argue that MWC 300 is most likely a binary system, because of the similarities of its observed parameters with those of recognized B[e] binaries.

Key words. stars: emission-line, Be – stars: individual: MWC 300 – techniques: spectroscopic – circumstellar matter – radiative transfer

1. Introduction

MWC 300 is one of the most controversial early-type emission-line stars. It was discovered during the Mount Wilson spectroscopic survey (Merrill & Burwell 1933). Merrill & Bowen (1951) noticed very bright forbidden lines of neutral oxygen (λ6300 Å and λ6363 Å) and measured a mean radial velocity (RV) of 13 emission lines of Fe II, [Fe II], and [S II] in the blue spectral region ($RV = 18.6$ km s^{-1}). Due to the presence of a nebulosity around the star, Herbig (1960) included it in his list of pre-main-sequence star candidates. Allen & Swings (1976) found a strong near-IR excess due to circumstellar (CS) dust in MWC 300 and listed it as a B[e] star. Appenzeller (1977) found absorption lines of He I, He II, O II, and C III in a low resolution spectrum and classified the object as a B1 Ia supergiant.

MWC 300 is a strong source of mid- and far-IR radiation. It was detected in all 4 IRAS bands with comparable fluxes at 12 and 25 μm (~100 Jy) and lower fluxes at 60 and 100 μm. In the latter 2 bands the source appears extended. Both the low-resolution IRAS spectrum at 8–22 μm and the ISO spectrum at 2–45 μm show an absorption band near 10 μm. Molster et al. (2002) suggested that the band's profile might be a superposition of the interstellar (IS) absorption and CS emission. They also found dust features in the ISO spectrum at around 28.8 and 39.8 μm and attributed them to crystalline silicates.

First high-resolution spectrum of MWC 300 was obtained by Wolf & Stahl (1985, hereafter WS85). These authors noticed a few emission lines of Fe III (mult. 115 and 117), which seem to be only seen in the spectra of hypergiant B-type stars.

Send offprint requests to: A. S. Miroshnichenko,
e-mail: anatoly@physics.utoledo.edu

⋆ Partially based on observations collected at the Canada-France-Hawaii telescope (CFHT), operated by the National Research Council of Canada, the Centre National de la Recherche Scientifique, and Univeristy of Hawaii.

Based on this comparison, they estimated an absolute bolometric magnitude $M_{\rm bol} \approx -9.5$ mag and a distance $D \approx 15.5$ kpc. They concluded that MWC 300 is a massive (initial mass $M \sim 50\ M_\odot$) dusty B[e] supergiant, similar to such objects observed in the Magellanic Clouds (Zickgraf et al. 1986), and probably a runaway survivor of a supernova explosion in a binary system.

On the other hand, MWC 300 continued to be listed in catalogs of pre-main-sequence stars (e.g., Finkenzeller & Mundt 1984; Thé et al. 1994). Henning et al. (1994) noted that at $D = 15.5$ kpc the amount of CS gas around MWC 300, estimated from their 1.3 mm flux, might be unrealistically large ($\sim$300 $M_\odot$).

Pirzkal et al. (1997), Ageorges et al. (1997), and Leinert et al. (2001) have found no close near-IR companion to MWC 300 (down to $\sim$0.″4, 0.″2, and 0.″1, respectively). Leinert et al. (2001) detected a faint halo with a full width at half-maximum (*FWHM*) of 1.″1 ± 0.″3 and a flux of 0.07 ± 0.02 of the total flux in the *K* band (2.2 μm). Testi et al. (1998), who searched for clusters around young stars using near-IR imaging photometry, found a crowded field around MWC 300. The star density in its vicinity is similar to that around other early B-type Herbig stars. However, MWC 300 is located close to the galactic plane, and it is not clear whether these stars represent a cluster, or are distant but just close to it in projection on the plane of the sky.

Corporon & Lagrange (1999, hereafter CL99) obtained 7 high-resolution spectra of MWC 300 (with a resolving power $R \sim 48\,000$) in 1994−1997. They detected *RV* variations of both emission and absorption components of the He I lines at λ5876 Å and λ6678 Å and suggested that MWC 300 might be a binary system. In their spectro-astrometric observations of the star, Takami et al. (2003) detected a 17 ± 4 mas positional displacement of the central absorption feature of Hα with respect to the positions of other parts of the profile and the nearby continuum. They interpreted this result in terms of the presence of a stellar companion rather than of a jet or a wind. Combining the distance, deduced from the hypergiant classification (15.5 kpc), and an average mass of a Herbig Be star (5 $M_\odot$), they also estimated an orbital period of ≥2000 years and argued that the line profile variations reported by CL99 could not be explained by the orbital motion.

MWC 300 was extensively observed in 1984−1990 in the course of the Majdanak (Uzbekistan) program of the *UBVR* photometric monitoring of Herbig Ae/Be and related stars (Herbst & Shevchenko 1999). Only mild ($\Delta m \sim$ 0.15 mag) and irregular brightness variations were detected. The near-IR photometry (*JHKLM*), obtained in 1970−1989 and presented in several papers, shows the same variation level.

The above mentioned data are insufficient to draw any definite conclusion about the nature and evolutionary state of MWC 300. In the course of our studies of B[e] supergiant candidates, we undertook high-resolution spectroscopic observations of the object. In this paper we present and analyze them along with other similar data available to us. The observations are described in Sect. 2, our new results are presented in Sect. 3, our analysis of the observed properties is given in Sect. 4, and conclusions are summarized in Sect. 5.

Table 1. Log of high-resolution spectroscopic observations of MWC 300. Listed are the dates, exposure starting times (in MJD = JD−2 450 000), exposure time, signal-to-noise ratios (at 5900 Å for the red and at 5000 Å for the blue spectra), spectral region covered, and the observatories.

Date	MJD	Exp. s	Sp. region Å	*SNR*	Observatory
1998/07/04	998.755	900	3635–5425	20	Leoncito
1998/08/06	1031.698	1000	6345–8450	70	Leoncito
2000/06/25	1720.754	1000	3960–5925	40	Leoncito
2000/07/20	1745.675	3600	3870–5930	50	Leoncito
2000/07/21	1747.499	3600	5570–8415	60	Leoncito
2000/07/24	1749.662	3600	5570–8415	60	Leoncito
2001/09/08	2160.813	1800	6670–6753	90	CFHT
2001/10/11	2193.561	1800	5540–6950	70	McDonald
2002/05/28	2423.055	900	5660–5735	90	CFHT
2002/05/28	2423.055	900	6510–6625	70	CFHT
2002/06/23	2449.758	2000	5810–9020	70	Leoncito
2002/06/24	2450.810	1800	5810–9020	60	Leoncito

2. Observations

Most of our spectroscopic observations were obtained at the 2.1 m telescope of the Complejo Astronómico El Leoncito (Argentina) with the échelle spectrograph REOSC, mounted at the Cassegrain focus and equipped with a 2000 × 2000 pixel CCD chip. This setup allowed us to achieve $R \sim 15\,000$. One spectrum was obtained at the 2.1 m Otto Struve telescope of the McDonald Observatory (Mt. Locke, Texas) with the Sandiford échelle-spectrometer (McCarthy et al. 1993) with $R \sim 60\,000$ and a 1200 × 400 pixel CCD. Three spectra were taken at the 3.6 m CFHT (Mauna Kea, Hawaii) with the high-resolution ($R \sim 100\,000$) Gecko échelle spectrograph, fiber-fed from the Cassegrain focus (Baudrand & Vitry 2000), and a 2048 × 4608 × 13.5 μm^2 thinned back-illuminated EEV chip. The fiber was continuously agitated to overcome modal noise (Baudrand & Walker 2001). The log of our high-resolution spectroscopic observations is presented in Table 1. The data reduction was performed in IRAF[1].

Additionally, we used the high-resolution spectra obtained at ESO and Observatoire de Haute Provence (OHP), reported respectively by WS85 and CL99. Only the red part of the ESO spectrum (5730−6780 Å) is available to us, with a signal-to-noise ratio (*SNR*) of ∼70 near 5900 Å and $R \sim 30\,000$, obtained on August 31, 1984. The wavelength range of the OHP spectra is 3800−6815 Å. The OHP spectra were obtained on May 21, 1994, August 26, 1994, June 6, 1995, June 10, 1995, July 28, 1996, July 4, 1997, and July 7, 1997. Their mean *SNR* is ∼30, except for the spectrum of June 6, 1995, whose *SNR* is ∼50 near 5900 Å.

[1] IRAF is distributed by the National Optical Astronomy Observatories, which are operated by the Association of Universities for Research in Astronomy, Inc., under contract with the National Science Foundation.

The IR imaging was performed on October 22, 2001, at Mauna Kea with the 3 m NASA Infrared Telescope Facility (IRTF) and the IR camera MIRLIN. The camera has a 128 × 128 pixel, high-flux Si:AS BIB detector with a plate scale of 0.″475 at IRTF. Background subtraction was carried out by chopping the secondary mirror at an 11 Hz rate with a 15″ throw in the north-south direction and by nodding the telescope a similar distance in the east-west direction. The observations were obtained in the N (effective wavelength $\lambda_{\rm eff}$ = 10.79 μm and passband $\Delta\lambda$ = 5.66 μm) and Q_s ($\lambda_{\rm eff}$ = 17.90 μm and $\Delta\lambda$ = 2.00 μm) bands. Five cycles, each consisting of 25 co-added 50 chop pairs, were carried out in the N band. In the Q_s band we also took 5 cycles, each containing 20 co-added 100 chop pairs. Close standard stars HR 6869 and HR 7525 were observed before and after MWC 300.

The imaging data were reduced using an IDL package developed at Jet Propulsion Laboratory (Pasadena) for MIRLIN. The resultant image has a 32 × 32 pixel field. The total flux within the object's images was measured using the PHOT task under the APPHOT package in IRAF. The object's brightness was calibrated using known brightnesses of the standard stars in the N and Q ($\lambda_{\rm eff}$ = 20.8 μm, $\Delta\lambda$ = 1.7 μm) bands and in the IRAS 12 and 25 μm bands.

The infrared low-resolution spectroscopic observations were acquired on July 18, 2002 with the 3 m Shane reflector of the Lick Observatory and the Aerospace Corporation's Near-Infrared Imaging Spectrograph. The spectrograph, which is described by Rudy et al. (1999), uses two channels to provide wavelength coverage from 0.8 to 2.5 μm. The blue (0.8−1.4 μm, resolution 14 Å) and red (1.4−2.5 μm, resolution 36 Å) spectra were acquired simultaneously. A more detailed technical description of this type of observations is given in Miroshnichenko et al. (2000). A 2.″7 slit was employed for the observations of MWC 300 and its calibrator star HR 7034, an F7 dwarf (V = 6.31 mag). The instrumental response and most of the effects of atmospheric absorption were removed by dividing the spectra of the stars by that of the calibrator. To remove the intrinsic spectrum of the calibrator from this ratio, we used a model from Kurucz (1994) appropriate for an F7 V star.

3. Results

3.1. The spectrum

The spectroscopic data for MWC 300 that we have in our possession cover more than a decade of observation. The spectral line content is stable, but the lines are variable in both intensities and *RV*s. The *RV* variations have previously been reported by CL99 only for the He I 5876 Å line. We measured *RV*s of most unblended spectral lines, which were registered with a good SNR, by fitting a Gaussian to their profiles. The mean *RV*s of individual lines and their groups are presented in Tables 2 and 3. The mean measurement error of an individual line or of a line component position does not exceed 5 km s^{-1} in most cases.

Our measurements show a systematic difference in the line *RV*s from the OHP spectra with respect to those from the other observatories. The OHP line positions are blueshifted by 16 ± 3 km s^{-1} on average (see Table 2). Within the uncertainties, the shift is the same for all types of spectral lines (pure emission, pure absorption, and P Cyg type). It seems that this effect was taken into account by CL99 for the He I lines. We also corrected the OHP *RV*s for the average shift to create a homogeneous set of data.

Table 2. Average radial velocities of the spectral lines in the spectrum of MWC 300.

Line(s)	E/A	$\lambda_{\rm lab}$ Å	OHP km s^{-1}	N	Other km s^{-1}	N
[N II]	em	5754.80	−0.4 ± 1.6	6	+14.5 ± 2.0	6
[N II]	em	6548.10	+8.3 ± 5.0	5	+20.6 ± 1.5	6
[N II]	em	6583.60	+1.0 ± 2.0	6	+15.0 ± 1.4	6
Na I D2	em	5889.95	+15.8 ± 1.5	6	+36.7 ± 5.0	4
Na I D1	em	5895.92	+12.6 ± 2.3	4	+32.1 ± 2.4	3
Fe, Si II[a]	em		+11.6 ± 1.2	6	+25.6 ± 2.4	6
Fe III[b]	em		+16.0 ± 2.0	2	+31.3 ± 1.5	4
Hα [c]	em	6562.82	−38.2 ± 2.3	6	−27.2 ± 2.9	6
Hα [d]	em	6562.82	+34.8 ± 1.6	5	+51.7 ± 0.8	5
Hα [e]	abs	6562.82	−17.6 ± 1.3	6	−1.9 ± 1.6	6
DIB	abs	5780.41	−25.0 ± 2.5	3	−5.7 ± 2.2	4
DIB	abs	5797.03	−23.8 ± 2.3	4	−10.2 ± 1.5	5
DIB	abs	6613.62	−27.8 ± 2.6	3	−12.0 ± 2.0	6

The line identification is listed in Col. 1, the line type (absorption or emission) in Col. 2, the laboratory wavelength in Col. 3, the average *RV* in the OHP spectra and those from other observatories in Cols. 4 and 6, and the number of spectra taken into account in each data set in Cols. 5 and 7, respectively.

[a] 55 lines were used in each set of spectra.
[b] Only the lines at λ5999.30 Å and λ6032.30 Å with no contamination from other lines were taken into account.
[c] The blue emission peak.
[d] The red emission peak.
[e] The central depression.

3.1.1. Absorption lines

The pure absorption lines (Fig. 1) vary up to 40 km s^{-1} in *RV* and display clear signs of splitting. Our McDonald and CFHT spectra reveal weak blue components of some of the N II and Al III lines which are not seen in the OHP spectrum of 1995. The components' separation in N II λ5679.6 Å and Al III λ5696.5 Å line is 52 ± 2 km s^{-1} in our McDonald spectrum. It is 46 ± 1 km s^{-1} for N II λ5679.6 and λ5686.2 Å lines in the CFHT spectrum. Such a splitting is observed in the spectra of some super- and hypergiants (e.g., Chentsov et al. 2003). The blueshifted weak absorption components may arise in the densest regions of the CS envelope near the stellar surface. The splitting may also be due to a narrow emission component within the absorption profile. In fact, the maximum intensity in the splitted profiles is near the mean *RV* of the single-peaked emission lines (see Fig. 1 and Sect. 3.1.2). Unfortunately, not all the spectra have high SNR, which hampers higher quality

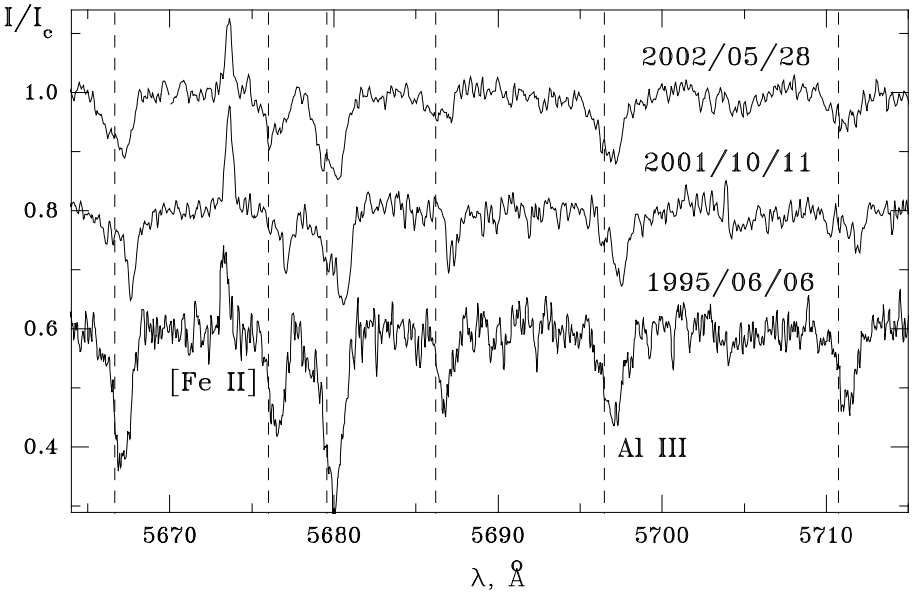

Fig. 1. Portions of the spectrum of MWC 300 with photospheric lines. The vertical dashed lines show laboratory positions of N II (all unmarked lines) and Al III lines. The intensities are in continuum units, and the heliocentric wavelengths are in Å.

Table 3. Heliocentric radial velocities of the moving spectral lines in MWC 300. The *RV* of the He I 5876 Å line in the OHP spectra are taken from Table 3 of CL99. The average *RV* of the photospheric lines in the OHP spectra is corrected for a systematic shift (see text). *N* is the number of photospheric lines (O II, N II, Al III, and Si III) taken into account.

Date	Photospheric lines	*N*	He I abs. 5876 Å	He I emis. 5876 Å
1994/05/21			−36.3	+46.4
1994/08/26			−29.2	+49.9
1995/06/06	+42.5 ± 2.8	17	−43.9	+36.6
1995/06/10			−57.4	+37.0
1996/07/28			−39.4	+42.0
1997/07/04	+60.5 ± 0.3	2	−16.7	+60.5
1997/07/06			−25.0	+61.1
2000/06/25	+70.0	1	−36.3	+57.1
2000/07/21			–	+42.9
2000/07/24	+32.9 ± 4.0	5	−47.2	+32.9
2001/10/11	+52.7 ± 3.2	6	−46.4	+45.4
2002/05/28	+33.9 ± 2.9	6		
2002/06/23			−41.5	+38.6
2002/06/24			−41.1	+53.4

RV measurements. Also, individual *RV*s of the line components are somewhat uncertain, as they cannot be completely separated even at $R \sim 100\,000$.

Most of the detected pure absorption lines are strong, as was previously reported by WS85. Our data confirm the conclusion of these authors that strengths of the N II, O II, and Al III lines in the spectrum of MWC 300, which are luminosity-dependent in the spectra of normal stars and of those with a weak line emission, are reminiscent of super- and hypergiants. On the other hand, no obvious signs of the He II 4686Å line, whose presence was reported by Winkler & Wolf (1989), are seen neither in the OHP nor in the Leoncito blue spectra (see Fig. 3). The λ4686 Å line may be undetected because of the low *SNR*, while the absence of the λ5412 Å line (where the *SNR* is higher) is much better established.

The absorption-line spectrum of MWC 300 (strong lines of N II, O II, Al III, and Si III and the absence of C III lines) also indicates that its effective temperature $T_{\rm eff}$ is closer to 20 000 K rather than to 30 000 K. The He II line may, therefore, be transiently seen and may belong to a hotter secondary companion.

To make use of our equivalent width (*EW*) measurements of absorption lines, we collected *EW*s of photospheric lines of other early B-type stars in a wide luminosity range available in the literature (e.g., Gies & Lambert 1992). Direct comparison can be made only assuming that the lines are purely photospheric. The results, some of which are shown in Fig. 2, suggest that the luminosity of MWC 300 is $\log L/L_{\odot} = 5.1 \pm 0.1$. Nevertheless, some lines (e.g., O II λ4649 Å) are extremely strong, suggesting that either the element abundances of MWC 300 exceed average values in the supergiant atmospheres or the line strengths are affected by a variable CS contribution. It is seen in Fig. 1, that the absorption lines in the OHP spectrum of June 6, 1995 (also shown in Fig. 3) are noticeably stronger than those in the other spectra. This spectrum is the only source of our *EW*s in the blue region, all the others have too low *SNR* to derive reliable line parameters. A comparison of the spectrum of MWC 300 with those of supergiants was presented by WS85. The spectra are indeed very similar, and we do not repeat such a comparison here.

Thus, the basic stellar parameters derived here suggest that MWC 300 is less luminous than it has been previously thought. Assuming that it is a single star and using the evolutionary

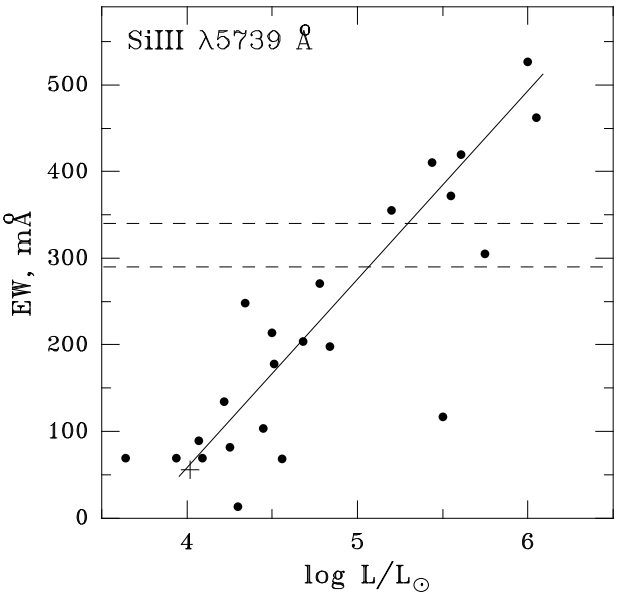

Fig. 2. Relationship between the *EW* of the Si III λ5739 Å line and stellar luminosity. A linear fit to the data is shown by the solid line. The parameters of the Herbig Be star HD 53367 are shown by the cross. The dashed lines represent extremal values of the line *EW* derived from our spectra of MWC 300.

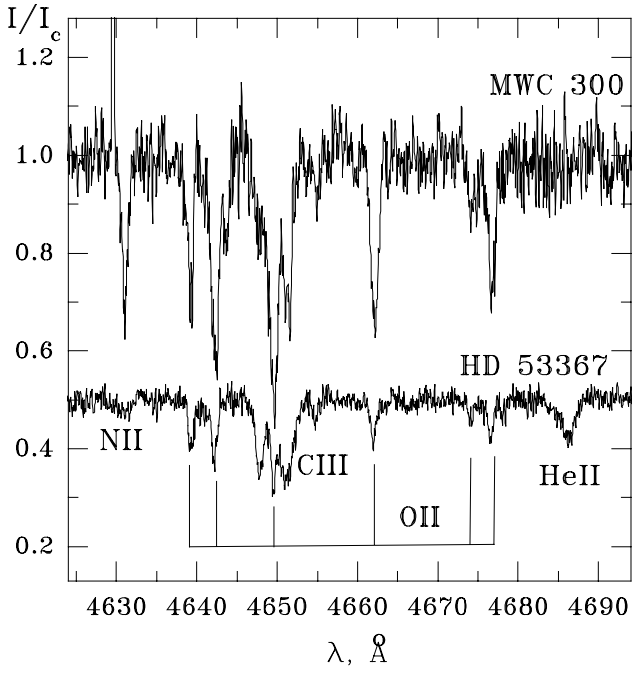

Fig. 3. Comparison of the spectra of MWC 300 and HD 53367. Lines of C III are blended with those of O II in the spectrum of HD 53367. The spectrum of HD 53367 was obtained on November 17, 1994, and the spectrum of MWC 300 on June 06, 1995 at OHP (from the data base of CL99). The intensities and wavelengths are in the same units as in Fig. 1.

tracks of Schaller et al. (1992), we can estimate its initial mass as ~20 $M_\odot$.

The diffuse IS bands (DIB) are moderately strong in the spectrum of MWC 300. They have single-peaked and

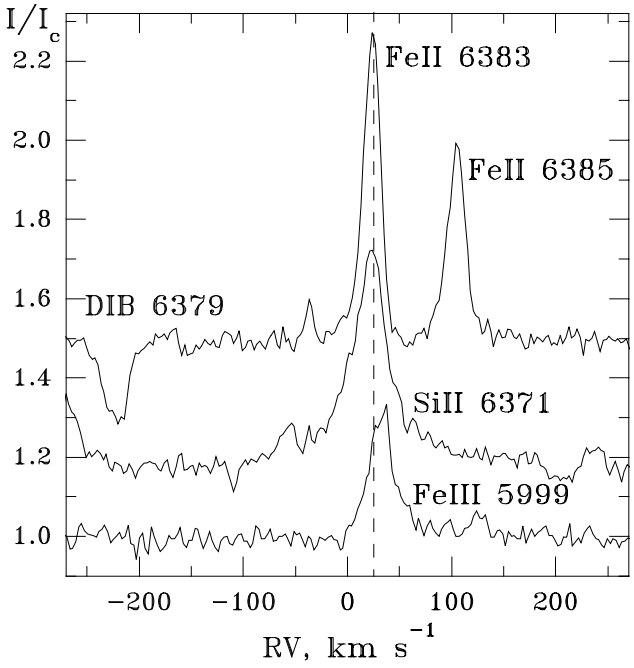

Fig. 4. Sample profiles of the emission lines from the McDonald spectrum of October 11, 2001. The dashed vertical line shows the average *RV* of symmetric emission lines (e.g., Fe II, Si II). The intensities are in continuum units, and the heliocentric *RV*s are in km s^{-1}.

nearly Gaussian profiles with a mean heliocentric radial velocity (*HRV*) of -10 ± 3 km s^{-1}, averaged over all the spectra. We used calibrations of Herbig (1975, 1993) to estimate the IS contribution to the object's reddening from reliably measured *EW*s of the DIBs. The average *EW*s of 0.44 ± 0.02 Å at λ5780 Å, 0.13 ± 0.02 Å at λ6379 Å, and 0.23 ± 0.03 Å at λ6613 Å correspond to $E(B-V) = 0.84 \pm 0.02$ mag. Another strong DIB with an *EW* of 0.22 ± 0.01 Å at λ5797 Å gives a much larger $E(B-V) = 1.47$ mag, according to Herbig (1993). The *EW* ratio of the DIBs at λ5797 and 5780 Å (0.5) is similar to those in the spectra of reddened stars in this part of the sky. However, it varies significantly from region to region, and use of the average relationship may be unreliable. The $E(B-V) = 0.84$ mag, derived from the DIBs, is significantly smaller than the photometric estimate (1.19 mag, WS85), and may imply a CS contribution to the overall reddening. On the other hand, as we show in Sect. 3.5.2, the strength of the silicate absorption feature near 10 μm seen in the ISO spectrum is more consistent with the photometric reddening estimate.

3.1.2. Emission lines

The data from Table 2 show that the pure emission lines did not change their positions during the last decade. Their profiles are mostly single-peaked and symmetric, except for the unblended Fe III lines at λ5999 Å (Fig. 4) and λ6032 Å. They also do not move and have an average *RV* a few km s^{-1} larger than the other emission lines. As seen in Fig. 4, the Fe III line profile has its blue part depressed that may cause the redshift. Nevertheless, the constant position of these lines implies that they are formed in the CS environment and not in the photosphere, as was

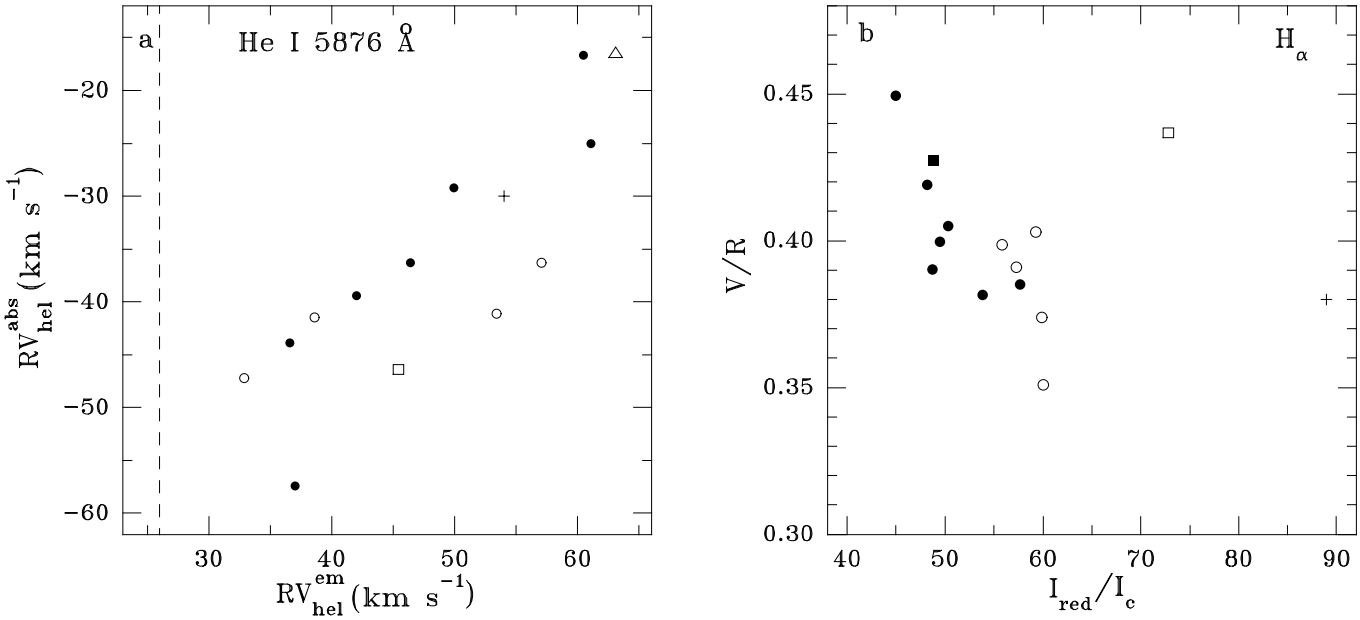

Fig. 5. Characteristics of emission lines in the spectrum of MWC 300. Panel **a)** shows the relationship between the *RV*s of the absorption and emission component of the He I λ5876 Å line. The vertical dashed line represents the mean position of the single-peaked emission lines (Fe II, Si II, etc.). Panel **b)** shows the relationship between the peak intensity ratio and the strength of the red peak of the Hα line. Data from different observatories: filled circles – OHP, open circles – Leoncito, open square – McDonald, filled square – CFHT, open triangle – ESO, crosses – data from Zickgraf (2003). The *RV*s are heliocentric, and the intensities are in continuum units.

suggested by WS85. At the same time, the *FWHM* of the Fe III lines is larger than those of Fe II lines and is comparable to those of Si II λ6347 and λ6371 Å lines. As WS85 pointed out, this indicates that the Fe III and Si II lines at least partly originate in a different CS zone than the Fe II lines.

The forbidden [O I] lines at λ6300 and λ6363 Å are extremely strong in the spectrum of MWC 300. Their average strengths in units of the underlying continuum are $I/I_c \sim 22$ and ~8, respectively. Their mean *EW* ratio, 2.97 ± 0.04, is close to the theoretical value for radiative de-excitation rate. The moderately strong lines of [N II] at λ6548 and λ6583 Å have average $I/I_c \sim 1.6$ and ~2.6, respectively, and a mean *EW* ratio of 0.3 ± 0.1. No [S III] λ6312 Å line is present in the spectrum. The maximum density of the CS gas in the formation region is $\sim 10^6$ cm^{-3} from the [O I] lines and $\sim 10^5$ cm^{-3} from the [N II] lines (Osterbrok 1989). These regions seem to be far away from the star and have a small velocity gradient, as the lines are narrow (*FWHM* ~ 25 km s^{-1}).

Despite the positional stability, all the emission lines vary in strength and *EW*. An average variation of the line *EW*s is 10% which may be caused in part by a low *SNR* of some spectra.

The Hα line has a double-peaked profile with the red peak stronger than the blue one. The peak intensity ratio (V/R = 0.40 ± 0.03) and their separation (75 ± 2 km s^{-1}) were almost constant over the last decade, despite a strong change in the intensities (Fig. 5b). The peak strengths in the ESO 1984 Hα profile are significantly lower and closer to each other ($I_{red} = 25.4\, I_{cont}$, $V/R = 0.75$) than in all the other profiles. The Hα *EW* varies between 95 and 157 Å with no obvious signs of periodicity. At the same time, the positions of the emission peaks and central depression were stable.

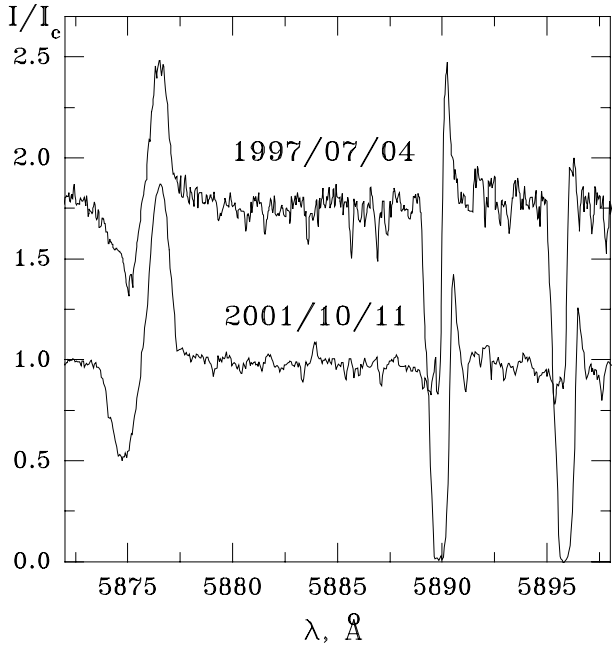

Fig. 6. Portions of the spectrum of MWC 300 with He I λ5876 Å and Na I D lines. The intensities and wavelengths are in the units of Fig. 1.

3.1.3. Lines with absorption and emission components

The Na I D lines at λ5889 and λ5895 Å show both absorption and emission components. The absorption component is saturated in the highest resolution spectra (such as our McDonald spectrum) and is most likely of IS origin. In some OHP spectra it is split into 2 sub-components at −28 and −8 km s^{-1}, which is not detected in the McDonald spectrum (Fig. 6). This may

be an instrumental effect. The average *RV* of the D lines in most of the spectra is -6 ± 2 km s^{-1} (in this estimate, only single absorption components and the redshifted sub-components were taken into account). In two spectra (OHP May 21, 1994 and Leoncito July 21, 2000), where only one absorption component is observed, *RV* is -19 km s^{-1}. This value may be an average of those of the two unresolved sub-components. In any case, the *RV* variation of the D lines is much smaller than that of the He I lines, thus not supporting the suggestion of CL99 about a correlation between the two. The emission components of the D lines are weak and positionally stable as well. Their mean *RV*s are slightly larger than those of single-peaked emission lines which may be due to the distortion by the IS components.

The *RV* variations of the absorption and emission component of the He I 5876 Å line correlate with each other (see Fig. 5a). Their amplitude is about 30 km s^{-1}, and there is no temporal trend. Our data are insufficient to draw any conclusion about periodicity of these variations. CL99 mention that the absorption component of the He I lines is supposed to be photospheric. It does not seem to be the case, because this component is significantly blueshifted with respect to the photospheric lines (see Table 3). It is more likely that the He I lines have P Cyg type profiles. They are thought to be formed near the stellar surface, where the CS density is the highest. Although the CS envelope of MWC 300 seems to be non-spherical, it is viewed close to edge-on (see Sect. 4) and contains enough matter in the line of sight to produce the strong P Cyg type absorption feature. Parameters of both the photospheric and He I lines were measured simultaneously in only 6 spectra (Table 3). The amplitudes of their *RV* variations are similar, and a correlation between the *RV*s is clearly seen despite the data sparseness.

3.2. Luminosity, distance, and reddening

The *RV* of the stationary single-peaked emission lines ($+26 \pm 2$ km s^{-1}) provides an estimate of the object's systemic velocity. Assuming that it is due to the galactic rotation, one can derive a distance $D = 1.8 \pm 0.2$ kpc toward MWC 300 (Dubath et al. 1988). Such a short distance is also supported by reddenings of projectionally close stellar groups (e.g., Sct OB2: $D = 1.9$ kpc, $A_V = 3.4 \pm 0.4$ mag and Ser OB2: $D = 1.0$ kpc, $A_V = 2.8 \pm 0.3$ mag, Humphreys 1978). Furthermore, the Wolf-Rayet star WR 117, located within 0.°7 from MWC 300 at $D = 3.0$ kpc, has a reddening of $E(B-V) = 1.56$ mag (van der Hucht 2001) which is larger than that of MWC 300. These data imply that there is enough IS dust within the local and Sagittarius spiral arms to produce the reddening, which may explain the observed optical color indices of MWC 300. At $D = 1.8$ kpc and the galactic latitude $b = 2.1°$, the distance of MWC 300 from the galactic plane would be only ~50 pc. Thus, the suggestion of WS85 about the runaway nature of the object becomes unnecessary.

The luminosity of MWC 300 ($\log L/L_\odot = 5.7$) was estimated by WS85, who assumed that the Fe III emission lines originate in the star's atmosphere. WS85 also mentioned that the strong absorption-line spectrum of MWC 300 indicated a high luminosity, but they presented no estimate based on the line strengths. As we show in Sect. 3.1, the Fe III lines arise in the CS medium. Therefore, the mechanism of their formation is different from that in the hypergiant atmospheres, and the analogy with their spectra does not provide a reliable luminosity for MWC 300.

Our luminosity estimate (4 times less than that of WS85, see Sect. 3.1.1) is based on the mean strength of the absorption lines. It does not take into account possible CS veiling and, in combination with our distance estimate, implies the presence of a significant extinction due to CS dust (see Sect. 3.5). In Sect. 3.5.2 we show that the observed spectral energy distribution (SED) can be closely fitted with both our luminosity and distance and discuss how the latter affect CS dust parameters.

3.3. Near-IR spectrum

Near-IR spectrum of MWC 300 was only published by Hamann & Persson (1989), who also identified spectral lines in the 7550−9300 Å region. Although obtained with a lower resolution, our Lick data demonstrate that the spectrum shows no significant changes in the overlapping region. For example, the *EW* of the O I λ8446 Å line is the same as that reported by Hamann & Persson (1989). The main spectral content in the 0.8−2.5 μm range is hydrogen, Fe II, and C, N, and O I lines. The He I λ10830 Å line is seen in emission. The lines detected and identified in our Lick spectrum are listed in Table 4. Portions of the spectrum are shown in Fig. 7.

The absolute fluxes are in very close agreement with the published photometric data (see Fig. 8). Our near-IR spectrum constrains the onset of the CS dust emission ($\lambda \sim 1.5$ μm) and joins the ISO data at its red edge. We also estimated the IS reddening using the flux ratio of the O I lines at λ8446, 11287, and 13164 Å (see Rudy et al. 1991 for the method). The resulting $E(B-V) = 0.66 \pm 0.25$. The large uncertainty is due to a complicated correction of the λ11287 Å line for the atmospheric transmission. Thus, the result is in agreement with the reddening estimate from both the DIBs and optical color-indices.

3.4. IR imaging and photometry

Our MIRLIN data show that the brightness of MWC 300 is -0.90 ± 0.03 mag in the *N* band and -2.30 ± 0.02 mag in the Q_s band. As seen in Fig. 8, our photometry is in good agreement with previously published data obtained both from ground and space.

MWC 300 shows no extension in comparison with point sources (the standard stars) in both images. The full width at half maximum (*FWHM*) is 1.″13 in the *N* band and 1.″55 in the Q_s band. In comparison, an *N*-band image of HR 6869, which was observed at the same air mass ($X = 1.4$) 10 min before MWC 300, has a *FWHM* of 1.″16. Another standard star, HR 7525, was observed 20 min after MWC 300 at $X = 1.12$ and have a *FWHM* of 1.″0 in the *N* band and 1.″43 in the Q_s band.

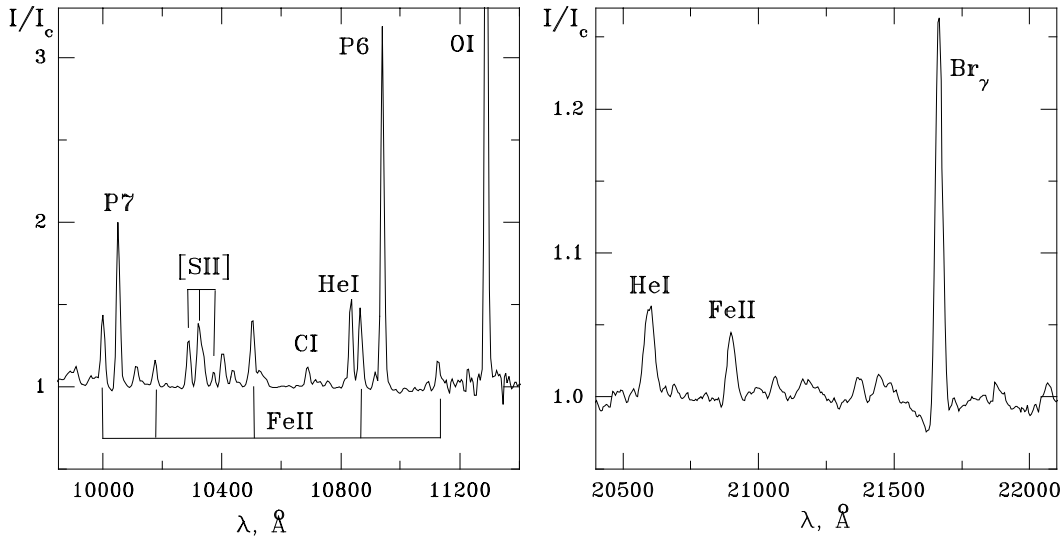

Fig. 7. Portions of the near-IR spectrum of MWC 300. Intensities are normalized to the underlying continuum.

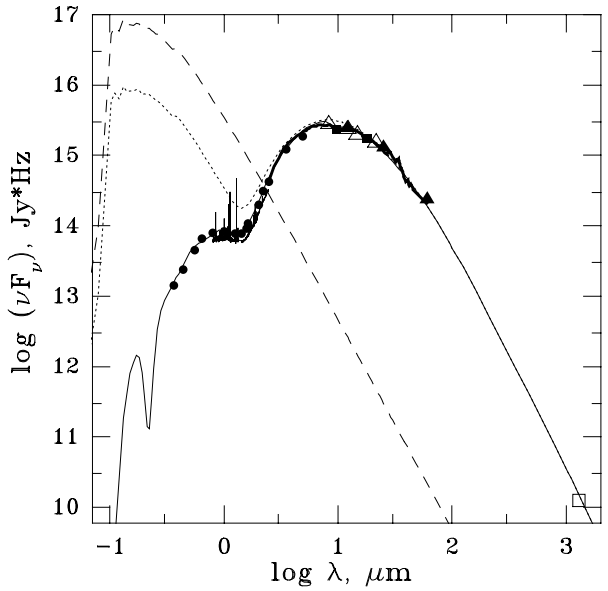

Fig. 8. Comparison of our 2D radiative transfer model of MWC 300 with the observed SED. The model SED (thin solid line) was corrected for the IS extinction. The model fluxes without the IS extinction are also shown (dotted line). These two SEDs merge at $\lambda \geq 30$ μm. The ground-based data are shown by filled circles, our IRTF data by filled squares, the MSX data by open triangles, the IRAS data by filled triangles, the ISO data by a thick solid line, and the submillimetric data from Henning et al. (1994) by an open square. The dashed line represents the Kurucz (1994) theoretical SED for the star ($T_{\rm eff}$ = 19 000 K, $\log g$ = 2.5). Refer to Sect. 3.5.2 for the model parameters.

3.5. Spectral energy distribution

We attempted to model the object's SED using two radiative transfer codes, which employ different geometries of the CS dusty envelope. The 1D code DUSTY (Ivezić et al. 1999) assumes a spherical envelope and a single (average) dust component, whereas our 1D/2D code (Men′shchikov & Henning 1997) employs a disk-like density distribution and an arbitrary number of dust components and grain sizes. Below we describe the results of our SED modelling using these two codes.

The observed SED was compiled using both ground- and space-based data. They include the average *UBVR* magnitudes from the database of Herbst & Shevchenko (1999), *JHKLM* photometry from Bouchet & Swings (1982) and Berrilli et al. (1992), our IRTF and Lick data, MSX photometry in range 3−21 μm (Egan et al. 1999), and IRAS photometry and low-resolution LRS spectrum. We used only a few data points from our near-IR spectrum to constrain the turnover wavelength near 1.5 μm. The IRAS 100 μm flux was not used for the modelling because the corresponding beam was very large, and thus it most likely contains a contribution from other sources. The ISO data were taken from Molster et al. (2002), and the flux at 1.3 mm is from Henning et al. (1994). As seen in Fig. 8, the measurements from different sources agree well with each other. The shape of the SED of MWC 300 is thus very well constrained.

Although some dust emission features are seen in the ISO spectrum of MWC 300 (Molster et al. 2002), their carrier and optical properties are not known, and therefore we ignored them in the present modelling of the global structure and properties of the CS environment of this object. We used optical properties of amorphous carbon (Preibisch et al. 1993) having a featureless continuum.

3.5.1. Spherical dusty envelope

The code DUSTY computes transfer of radiation in spherical dusty envelopes. In our modelling, the radiation of the central star was described by a stellar atmosphere model with $T_{\rm eff}$ = 19 000 K and $\log g$ = 2.5 (Kurucz 1994). The adopted gravity does not affect the results, as it only weakly changes the stellar SED at short wavelengths, outside of the range of our interest. The radial dust density distribution was described by a power-law $\rho \propto r^{-p}$, with the inner boundary at the dust sublimation

Table 4. Spectral lines idenitified in the near-IR spectrum of MWC 300.

ID	$\lambda_{\rm lab}$ Å	EW Å	$I/I_{\rm c}$	ID	$\lambda_{\rm lab}$ Å	EW Å	$I/I_{\rm c}$
O I	8446.35	29.1	2.50	N I	12 382.63	1.1	1.09
N I[a]	9386.81	8.0	1.35	N I[d]	12 461.30	3.9	1.18
P 8	9545.97	9.0	1.47	P 5	12 818.05	81.8	7.67
O I	8446.35	29.1	2.50	N I	12 382.63	1.1	1.09
N I[a]	9386.81	8.0	1.35	N I[d]	12 461.30	3.9	1.18
P 8	9545.97	9.0	1.47	P 5	12 818.05	81.8	7.67
Fe II	9997.56	6.0	1.43	[e]	13 083.2⋆	2.4	1.13
P 7	10 049.38	14.2	2.00	O I	13 164.1	7.7	1.55
Fe II	10 173.91	2.5	1.16	Br 16	15 556.45	3.0	1.04
[S II]	10 286.73	4.3	1.27	Br 15[f]	15 700.66	–	1.06
[S II][b]	10 320.49	8.8	1.38	Br 14	15 880.54	3.0	1.07
[S II]	10 370.50	1.2	1.09	Br 13	16 109.31	3.4	1.08
N I	10 399.59	3.8	1.20	Br 12	16 407.19	7.0	1.12
Fe II	10 501.00	7.0	1.40	Br 11[g]	16 787.18	11.1	1.21
C I[c]	10 688.1⋆	2.2	1.12	Fe II	16 873.19	8.0	1.21
He I	10 830.34	8.4	1.53	Br 10[g]	17 362.11	9.6	1.19
Fe II	10 862.64	7.9	1.48	Fe II	17 414.01	6.6	1.15
P 6	10 938.09	30.6	3.19	He I	20 581.28	2.8	1.06
Fe II	11 125.58	2.6	1.15	Fe II	20 888.10	1.6	1.05
O I	11 287.00	52.2	4.81	Br γ	21 665.29	8.2	1.26

⋆ The observed wavelength is listed.
[a] Possible blend with a N I line at λ9392.79 Å.
[b] Blend with a [S II] line at λ 10336.41 Å.
[c] A group of unresolved C I lines at $\lambda\lambda$ 10683–10707 Å.
[d] Blend with a N I line at λ12470.74 Å.
[e] Unidentified, but seen in other sources (Rudy et al. 2001).
[f] Blend with a stronger line at λ15575 Å.
[g] Blend with Fe II lines.

radius R_1. In this 1D modelling, we adopted average grains of the MRN grain size distribution (Mathis et al. 1977).

The power-law index p, the dust condensation temperature T_1, the V-band optical depth τ_V, the outer boundary $R_{\rm out}$ of the envelope, and the IS extinction $A_{\rm V}$ are free parameters of the model. Good fits of the observed SED were obtained for the following free parameters: $p = 1.55 \pm 0.05$, $T_1 = 650 \pm 50$ K, $R_{\rm out}/R_1 = 1600 \pm 100$, $R_1 = 670 R_\star$, $\tau_V = 1.3 \pm 0.1$, and $A_{\rm V} = 3.7 \pm 0.1$ mag. The mean r.m.s. deviation of the fit from the observed SED was ∼15%. The spherical fit is not shown in Fig. 8, as it is qualitatively the same as our 2D fit described in Sect. 3.5.2.

We did not try to find a very precise fit of the observed fluxes, since both the geometry and chemical composition of the dusty envelope are uncertain. Instead, we intended to estimate a possible CS attenuation of the star's radiation in the extreme spherical case. Optical depth of a flattened envelope producing the same amount of IR emission would be larger. The resulting model $A_{\rm V}$, which is the same as that estimated from the color indices, implies that the additional wavelength-dependent CS reddening is offset by the additional CS scattering into our line of sight.

The hottest dust is located at $\sim 5 \times 10^{15}$ cm from the star, if we adopt our luminosity estimate (Sect. 3.1.1). From our distance estimate (Sect. 3.2), we can derive angular size (∼0.″2) of that region, consistent with that of the halo detected by Leinert et al. (2001). The effective size of the CS dust at 10 and 20 μm is then less that 1″, also in agreement with our IRTF data.

Nevertheless, there is an obvious contradiction between our luminosity and distance estimates for MWC 300. The average brightness of the object ($V = 11.6$ mag) and its IS and CS reddening imply that at $D = 1.8$ kpc it would have $\log L/L_\odot = 4.6$, i.e. ∼3 times fainter than its absorption-line spectrum suggests. A larger CS extinction, which is ∼1.4 mag in the spherical case, can resolve the problem. Like the gaseous envelope of MWC 300, its dusty envelope is most likely flattened. Thus, the dust optical depth in the line of sight can be increased without significantly altering of the theoretical SED. We explore the non-spherical case in the next section.

3.5.2. Flared dusty disk

Although the spherical model of MWC 300 (Sect. 3.5.1) can fit the shape of the observed SED, the observed fluxes imply either a lower luminosity of the central star or a larger distance toward the object (at least by factors of ∼3 and ∼2, respectively). We believe that this discrepancy is just another indication of a significant deviation of the density distribution in the CS envelope of MWC 300 from spherical geometry, as suggested by the emission line profiles (cf. Sect. 4.2).

Our 2D model of MWC 300 is a relatively thin disk viewed through its edge (not exactly edge-on); there is no dust above and below the disk surfaces. The disk density distribution is essentially a 1D function of the radial distance from the central star, $\rho(r)$. The disk height is also proportional to r, so that the upper and lower disk surfaces have shapes of a cone with the origin at the center of the star. The full opening angle of the disk (between the upper and lower surfaces) in our final model was fixed at 30° and the disk inclination to the line of sight was assumed 10°. This disk geometry is basically the one adopted by Men′shchikov & Henning (1997, Fig. 1) in their radiative transfer method.

The dusty disk consists of amorphous carbon dust grains with a size distribution $\mathrm{d}n/\mathrm{d}a \propto a^{-3.3}$ for grain radii $0.5\,\mu\mathrm{m} < a < 1000\,\mu\mathrm{m}$. Shifting the size distribution to large grains was required primarily to fit the high observed flux at λ 1.3 mm and to produce an almost gray CS extinction in the optical and mid-IR region; otherwise small grains produce too much reddening at optical wavelengths.

The simplest possible dust model was adopted, since no reliable information on the dust properties in MWC 300 is available. The extinction due to IS dust was taken into account by reddening the model fluxes using the analytic fits by Cardelli et al. (1989), extended to λ 100 μm using data from Savage & Mathis (1979), and parameters $R_V = 3.1$ and $n_{\rm H} = 1.28$ cm^{-3}. The latter corresponds to the best-fit $A_{\rm V}$ at the chosen D (see below).

The other physical parameters of the disk model are D = 1.8 kpc, $L = 10^5\ L_\odot$, $T_{\rm eff}$ = 19 000 K, $R_\star = 29\ R_\odot$, $R_1 = 147 R_\star$, $R_{\rm out}/R_1 = 2000$, $T_1 = 1120$ K, $\tau_V = 3.0$ (in the disk equatorial plane), and $A_{\rm V} = 3.76$ mag. The total mass of gas and dust in the disk is $0.08\,M_\odot$, assuming the dust-to-gas mass ratio of 0.005. The density distribution smoothly changes from $\rho \propto r^0$ at the inner boundary to $\rho \propto r^{-4}$ at $r = 50\,R_1$, with 90 % of the total mass contained within $r = 200\,R_1$. The steep radial density profile, making the location of the outer boundary unimportant, is required by the model to reproduce the slope of the SED of MWC 300 between 50 μm and 1.3 mm.

The numerical model included 108 radial zones, 8 angular zones for the integration of the mean intensity, 50 angular zones for the observations of the converged model, and 125 frequencies (see Men′shchikov & Henning 1997 for details). The grain size distribution was binned into 19 representative grains. The iterations were terminated when relative corrections to all variables were below 0.1% and the total energy was conserved to within 2.6% at the outer boundary of the disk.

The 2D modelling results are shown in Fig. 8 in terms of the model SED compared to the observed flux distribution. There are no spatial constraints from resolved images, neither at high nor low angular resolution, which would otherwise enable us to derive a very well constrained and reliable model for this object. The disk model produces an extremely good fit to the SED of MWC 300 in the entire range from the UV to millimeter wavelengths, resolving the inconsistency between the relatively short distance and very high luminosity, existing in spherical geometry. The peak fluxes in an equivalent spherical model are 17 times higher than the observed IR fluxes. Most of the radiation from the central star escapes into the polar directions above the disk surfaces and therefore is lost for an observer.

Stellar radiation is attenuated by the relatively large CS grains producing $\tau_V = 3$. However, it is the IS extinction by small dust grains ($A_{\rm V} = 3.76$ mag) which defines the shape of the model SED at all wavelengths below ~30 μm. Since the 10 μm absorption feature is produced by IS dust extinction, at least to a large extent, there is no reason to include amorphous silicate grains in the model. Small carbon grains of the IS medium produce a very deep absorption feature at 0.22 μm. There are no observations of MWC 300 in the far UV, and any new (spectro)photometry would be very useful in testing this prediction of our model.

The model can be easily scaled with distance: the stellar luminosity and the disk's mass are proportional to D^2, the radii are proportional to D, and the dust density scales as D^{-2}. In other words, usually we cannot constrain distance from radiative transfer modelling of CS dusty envelopes. For a larger distance, our disk-like configuration must be geometrically thicker (more massive) in order to produce higher IR fluxes that would compensate for the observed flux decrease with distance. A significantly larger IS extinction would make the short-wavelength SED steeper and the 10−μm silicate absorption feature deeper. A lower CS optical depth would affect the theoretical SED the same way.

Alternatively, for a shorter distance the model configuration must be even thinner (geometrically) than the present, already rather thin disk, to reproduce the observed IR fluxes. The IS extinction would have a less pronounced influence on the model SED, so the model envelope must be adjusted to produce a steeper short-wavelength SED and a deeper silicate absorption feature. The latter would require an addition of silicates to the dust mixture, which implies a number of extra free model parameters. A larger optical depth would need an additional contribution of small particles that are likely to make worse both the short-wavelength and the long-wavelength fit to the observed SED.

Overall, our extensive modeling shows that the present model parameters give a very good fit to the entire observed SED, from the optical to the mm wavelengths. High-resolution imaging is needed to further constrain the CS envelope model parameters.

4. Discussion

Let us now discuss our findings described above, derive new estimates for the object's properties, and suggest follow-up observations to further improve our understanding of its nature and evolutionary state.

4.1. Evolutionary state

As we mentioned in Sect. 1, two very different evolutionary states have been proposed for MWC 300: a pre-main-sequence Herbig Be star and a post-main-sequence B[e] supergiant. The former one is mainly based on the presence of an optical nebulosity around the object and an estimate of the CS gas mass from the sub-mm flux. The latter hypothesis follows from the object's spectral classification (B1 Ia$^+$) and similarities of its observed properties with those of B[e] supergiants. Let us consider the evolutionary state of MWC 300 using the results of our study.

MWC 300 is very unlikely to be a pre-main-sequence star because of the following reasons.

1. The pre-main-sequence evolutionary time for an early B-type star is too short (~10^4 years, Palla & Stahler 1993) to get rid of the distant (and thus cold) protostellar dust. Observations of the most massive Herbig Be stars show that their IRAS fluxes at 60 and 100 μm are always larger than those at 12 and 25 μm.
2. Only the highest-temperature Herbig Be stars (e.g., HD 53367, B0, $T_{\rm eff} \sim 30\,000$ K) show noticeable absorption lines of O II, N II, etc. However, even these lines are much weaker than those in the spectrum of MWC 300 (Fig. 3) and obey the EW vs. luminosity relationships (Fig. 2).

On the other hand, our results for the luminosity and distance strongly suggest that MWC 300 is an evolved high-luminosity object, thus confirming the suggestions of Appenzeller (1977) and WS85. It is certainly not a post-AGB object because of its too high luminosity (cf., Blöcker 1995), but rather a massive system which has already passed the main-sequence phase. As theoretical calculations for massive binaries show (e.g., Kraicheva et al. 1977), primary components with initial masses

of $\gtrsim$20 $M_\odot$ may rapidly lose matter during the core helium burning stage and have characteristics of blue supergiants with altered abundances of hydrogen, helium, and CNO elements. This general picture is remarkably reminiscent of what we observe in MWC 300. We discuss evidence for the system binarity in Sect. 4.3.

4.2. Circumstellar envelope

The spectral line profiles and their *RV* variations suggest a complex structure of the gaseous CS envelope. The He I lines with P Cyg profiles are formed close to the envelope base and imply a large optical depth in the line of sight. The scale height should be high enough here to supress the blueshifted peak, which is characteristic of a very flattened geometry. On the other hand, the double-peaked profiles of the Balmer lines imply that the envelope is non-spherical. The large *RV* amplitude of both the photospheric and He I lines and the deep central depression of the Hα profile suggest that the envelope symmetry plane is viewed close to edge-on. Most of the single-peaked emission lines have symmetric profiles, indicating that they are formed in the optically-thin remote part of the envelope. That region is not very flattened, as the line profiles are not double-peaked, and is unaffected by the motion of the central object.

As our modelling shows, the dusty envelope is most likely non-spherical. It is compact and does not contain very cold dust ($\leq$100 K). These properties are consistent with its recent formation, indirectly supporting an evolved state of the object. If MWC 300 is a short-period binary (Sect. 4.3), the dusty envelope should be circumbinary. The single-peaked emission lines may also arise in the circumbinary area.

4.3. Evidence for binarity

No compelling evidence for binarity of MWC 300 has been found yet. The *RV* variations of the He I lines reported by CL99 and the displacement of the Hα central absorption observed by Takami et al. (2003) are only indirect signs of binarity. Our finding of the photospheric line *RV* variations makes the case stronger. However, the orbital period $P_{\rm orb}$ has yet to be found. Our spectroscopic data are insufficient to suggest even its order of magnitude. No set of the spectra obtained a few nights apart at both OHP and Leoncito allows us to measure short-term *RV* variations of the photospheric lines. The *RV* data for the He I line components (see Table 3) show that the position of one of them may vary up to 40% of the total amplitude in 1−2 days. This may indicate that $P_{\rm orb}$ is on the order of a few days. However, the component *RV* variations are not synchronous, which may be due to slightly different formation zones.

Nonradial pulsations (NRP), common in early-type emission-line stars, affect photospheric lines and may trigger discrete mass loss events. This mechanism may result in regular synchronous *RV* variations of both photospheric and CS lines with periods on a time scale of hours (up to 1−2 days), observed in some Be stars (e.g., Rivinius et al. 2001). To the best of our knowledge, NRP have not been detected in B[e] stars. Our data do not rule out nonradial pulsations as the cause of the *RV* variations in MWC 300. At the same time, the binary hypothesis cannot be ruled out either, because NRP is just a possible mass loss mechanism and can be present in binary systems (e.g., δ Sco, Smith 1986). The similarities in other observed object's properties (e.g., the strong emission-line spectrum, the IR SED shape, the presence of CS dust) to those of B[e] stars with detected secondaries (e.g., MWC 623, AS 381, V669 Cep, HDE 327083, see Miroshnichenko et al. 2002; and RY Sct, see below) make us believe that MWC 300 is most likely a binary system.

Other possible causes for the observed *RV* variations seem to be unlikely. For example, instabilities in the CS disk would not affect photospheric lines. Also, radial pulsations are not expected in such hot stars as MWC 300. Moreover, there is no evidence for them in the available extensive photometric data (377 observations during 6 years, Herbst & Shevchenko 1999).

Our *RV* data also show that both the photospheric lines and the emission component of the He I λ5876 Å line always have more positive *RV*s than the pure emission lines (see Fig. 5 and Table 3). The latter seem to be formed in the outer parts of the CS envelope not affected by the possible orbital motion. If the stationary emission lines represent the systemic velocity, then we should observe the photospheric lines at both positive and negative *RV*s with respect to this velocity. Possible explanations of this behaviour include an eccentric orbit and the data sparseness. Only additional high-resolution spectroscopy with $SNR \geq 70$ during several consecutive nights can resolve this problem.

Adopting our $D = 1.8$ kpc and a lower limit for the companion angular separation from Takami et al. (2003), 17 mas, one can estimate a linear separation to be 30 AU and $P_{\rm orb} \geq 48\,(25\ M_\odot/\Sigma M)$ years, where ΣM is the total mass of the system. This period is still too long to cause the observed *RV* variations. It is possible that Takami et al. (2003) found a more distant companion, which has a different strength of Hα and no effect on the observed *RV*s. A similar situation is observed in the Herbig Be star MWC 1080 where a very close unresolved companion causes photometric variations (Grankin et al. 1992) and a more distant one (at a separation of 2″) is seen in the IR region (Pirzkal et al. 1997). On the other hand, Takami et al. (2003) based their conclusion about the presence of a companion on analogy with binaries, where the displacement also occurs at only positive or negative *RV*s, but the deviating wavelength region is much wider. Also, they only compared the result with those expected from jets and winds and did not consider a disk, where the Hα line of MWC 300 seems to be formed. Moreover, the observed displacement is very small. Its detection may be spurious and needs further confirmation.

There are no signs of the secondary companion neither in the red and near-IR spectrum nor in the SED. This implies that, if it is a late-type star, it should be at least 3−4 mag fainter than the primary. However if the secondary causes the appearance of the He II λ4686 Å line (WS85), it could be an O-type star. In fact, MWC 300 might be similar to RY Sct, an eclipsing binary with late O-type or early B-type companions of a close brightness and an orbital period of ~11 days (see Smith et al. 2002 for the latest results). It has an emission-line spectrum,

reddening in the optical region, and IR SED similar to those of MWC 300. It is remarkable that Smith et al. (2002) found a systemic velocity of 20 km s^{-1} and $D = 1.8 \pm 0.1$ kpc, which are very close to our findings for MWC 300. Thus like RY Sct, MWC 300 may be a β Lyr binary, but with no eclipses.

If we assume that the observed *RV* amplitude is only half of the real amplitude (~80 km s^{-1}) and an orbital period of 10 days, the secondary's mass function would be 0.5 $M_\odot$. Assuming also an edge-on orbital orientation, a zero eccentricity, and the primary's mass of 20 $M_\odot$ (Sect. 3.1.1), the secondary's mass would be ~6 $M_\odot$. This estimate is not unreasonable for a β Lyr system and can be refined by follow-up spectroscopic observations.

5. Conclusions

Summarizing the results reported above, we can draw the following conclusions about the properties, nature, and evolutionary state of the emission-line object MWC 300.

1. Numerous high-resolution optical spectra of MWC 300 obtained in 1984−2002 show that most of the pure emission lines do not change their *RV*s with time. Neglecting some distortion effects, we conclude that all single-peaked emission lines have the same *RV* of 26 ± 2 km s^{-1} which may represent the systemic velocity.
2. The *RV* variation of the photospheric lines is detected for the first time. Its amplitude (~40 km s^{-1}) and temporal behaviour are similar to those of the emission and absorption component of the He I 5876 Å line.
3. The absorption-line spectrum indicates that MWC 300 has an early B-type spectral type and a high luminosity, thus supporting earlier suggestions by Appenzeller (1977) and WS85. Although our estimate of $T_{\rm eff}$ confirms the previous findings, the luminosity found in this work, $\log L/L_\odot = 5.1 \pm 0.1$, is lower than suggested before. It may be considered an upper limit, because of a possible CS contribution to the line strengths.
4. Adopting the mean *RV* of the single-peaked lines as a systemic velocity, we derive a distance $D = 1.8 \pm 0.2$ kpc for MWC 300 based on the galactic rotation curve. This relatively short distance is consistent with the object's brightness and luminosity only in the case of an optically-thick disk-like density distribution viewed relatively close to the edge-on orientation.
5. The detected *RV* variations may be due to either NRP or orbital motion in a binary system. We speculate that MWC 300 is a binary, because many of its observed characteristics are similar to those of recognized B[e] binaries.
6. The lack of cold dust in the vicinity of MWC 300 suggests either that the CS dust was formed recently or that it is located in a long-lived dusty circumbinary disk. A comparison with pre-main-sequence Herbig Be stars shows that MWC 300 must have a different evolutionary state.

The following observations need to be performed in order to place stronger constraints on the object's parameters. High-resolution spectroscopy on a time scale of hours-days is capable of refining the *RV* curve and answering the question about the cause of the *RV* variations (NRP or orbital motion). IR (speckle) interferometry at ~10 mas resolution could image the inner CS dusty environment and better constrain its geometry and size. Space-based UV spectroscopy could find signatures of the secondary companion.

Acknowledgements. A.M. and K.S.B. acknowledge support from NASA grant NAG5–8054 and thank the IRTF staff for their assistance during the observations. Karen Bjorkman is a Cottrell Scholar of the Research Corporation, and gratefully acknowledges their support. N.M. thanks the Executive Director of CFHT for granting discretionary telescope time. A.B.M. acknowledges support from the Natural Sciences and Engineering Research Council of Canada (NSERC). R.J.R., D.K.L., C.C.V., and S.M. were supported by the Independent Research and Development program at The Aerospace Corporation. We thank P. Corporon for making the OHP data available to us. This research has made use of the SIMBAD database operated at CDS, Strasbourg, France.

References

Ageorges, N., Eckart, A., Monin, J.-L., & Ménard, F. 1997, A&A, 326, 632
Allen, D. A., & Swings, J.-P. 1976, A&A, 47, 293
Appenzeller, I. 1977, A&A, 61, 21
Baudrand, J., & Vitry, R. 2000, in Proc. SPIE, 4008, 182
Baudrand, J., & Walker, G. A. H. 2001, PASP, 113, 851
Berrilli, F., Corciulo, G., Ingrosso, G., et al. 1992, ApJ, 398, 254
Blöcker, T. 1995, A&A, 299, 755
Bouchet, P., & Swings, J. P. 1982, Proc. IAU Symp., 98, 241
Chentsov, E. L., Ermakov, S. V., Klochkova, V. G., et al. 2003, A&A, 397, 1035
Cardelli, J. A., Clayton, G. C., & Mathis, J. S. 1989, ApJ, 345, 245
Corporon, P., & Lagrange, A.-M. 1999, A&AS, 136, 429 (CL99)
Dubath, P., Mayor, M., & Burki, G. 1988, A&A, 205, 77
Egan, M. P., Price, S. D., Moshir, M. M., et al. 1999, The Midcourse Space Experiment Point Source Catalog Version 1.2, Explanatory Guide, AFRL-VS-TR-1999-1522
Finkenzeller, U., & Mundt, R. 1984, A&AS, 55, 109
Gies, D. R., & Lambert, D. L. 1992, ApJ, 387, 673
Grankin, K. N., Shevchenko, V. S., Chernyshev, A. V., et al. 1992, IBVS, 3747
Hamann, F., & Persson, S. E. 1989, ApJS, 71, 931
Henning, T., Launhardt, R., Steinacker, J., & Thamm, E. 1994, A&A, 291, 546
Herbig, G. H. 1960, ApJS, 4, 337
Herbig, G. H. 1975, ApJ, 196, 129
Herbig, G. H. 1993, ApJ, 407, 142
Herbst, W., & Shevchenko, V. S. 1999, AJ, 118, 1043
Humphreys, R. M. 1978, ApJS, 38, 309
Ivezić, Ž., Nenkova, M., & Elitzur, M. 1999, User Manual for DUSTY, Univ. of Kentucky Internal Report, accessible at `http://www.pa.uky.edu/~moshe/dusty`
Kraicheva, Z. T., Tutukov, A. V., & Yungelson, L. R. 1977, Sov. Astron., 21, 61
Kurucz, R. L. 1994, Smithsonian Astrophys. Obs., CD-ROM No. 19
Leinert, C., Haas, M., Abraham, P., & Richichi, A. 2001, A&A, 375, 927
Mathis, J. S., Rumpl, W., & Nordsieck, K. H. 1977, ApJ, 217, 425
McCarthy, J. K., Sandiford, B. A., Boyd, D., & Booth, J. 1993, PASP, 105, 881
Men′shchikov, A. B., & Henning, Th. 1997, A&A, 318, 879
Merrill, P. W., & Burwell, C. G. 1933, ApJ, 78, 87

Merrill, P. W., & Bowen, I. S. 1951, PASP, 63, 295
Miroshnichenko, A. S., Chentsov, E. L., Klochkova, V. G., et al. 2000, A&AS, 147, 5
Miroshnichenko, A. S., Bjorkman, K. S., Chentsov, E. L., & Klochkova, V. G. 2002, in Exotic Stars as Challenges to Evolution, ed. C. A. Tout, & W. Van Hamme, ASP Conf. Ser., 279, 303
Molster, F. J., Waters, L. B. F. M., Tielens, A. G. G. M., & Barlow, M. J. 2002, A&A, 382, 184
Osterbrok, D. 1989, Astrophysics of Gaseous Nebulae and Active Galactic Nuclei (Mill Valley: Univ. Science Books)
Palla, F., & Stahler, S. W. 1993, ApJ, 418, 414
Pirzkal, N., Spillar, E. J., & Dyck, H. M. 1997, ApJ, 481, 392
Preibisch, Th., Ossenkopf, V., Yorke, H. W., & Henning, Th. 1993, A&A, 279, 577
Rivinius, Th., Baade, D., Štefl, S., et al. 2001, A&A, 369, 1058
Rudy, R. J., Erwin, P., Rossano, G. S., & Puetter, R. C. 1991, ApJ, 383, 344
Rudy, R. J., Puetter, R. C., & Mazuk, S. 1999, AJ, 118, 666
Rudy, R. J., Lynch, D. K., Puetter, R. C., Mazuk, S., & Derborn, D. S. P. 2001, AJ, 121, 362
Savage, B. D., & Mathis, J. S. 1979, ARA&A, 17, 73
Schaller, G., Schaerer, D., Meynet, G., & Maeder, A. 1992, A&AS, 96, 269
Smith, M. A. 1986, ApJ, 304, 728
Smith, N., Gehrz, R. D., Stahl, O., Balick, B., & Kaufer, A. 2002, ApJ, 578, 464
Takami, M., Bailey, J., & Chrysostomou, A. 2003, A&A, 397, 675
Testi, L., Palla, F., & Natta, A. 1998, A&AS, 133, 81
Thé, P. S., de Winter, D., & Pérez, M. R. 1994, A&AS, 104, 315
van der Hucht, K. A. 2001, New Astron. Rev., 45, 135
Winkler, H., & Wolf, B. 1989, A&A, 219, 151
Wolf, B., & Stahl, O. 1985, A&A, 148, 412 (WS85)
Zickgraf, F.-J., Wolf, B., Leitherer, C., Appenzeller, I., & Stahl, O. 1986, A&A, 163, 119
Zickgraf, F.-J. 2003, A&A, 408, 257